C h a p t e r   3

POLYHEDRAL SPECULAR REFLECTOR

The goal of the Full Spectrum Photovoltaics Project was to design and prototype a 50% module efficiency photovoltaic system. Of the three designs we initially pursued, the Polyhedral Specular Reflector (PSR) design came closest to achieving this goal. In targeting this efficiency record, our design evolved over time as we fleshed out our device models and gained new information.

The initial estimate from Emily Warmann's detailed balance modeling was that we would need to to incorporate eight single-junction III-V subcells for 50% efficiency. The initial design, shown in Figure 3.1a, was inspired by Reference [12]. Largely collimated light entered the device via a primary trough concentrator and hit a series of solar cells tiled along the sides of a parallelepiped angled at 45° to the direction of light incidence. It was noted that the lowest bandgap cell contributed only 0.5% of the power to the device, so it was decided to eliminate it and have a seven-way split instead. The 7th cell would be attached to the bottom of the parallelepiped instead of on the side. The bandgaps of the seven chosen subcells are listed in Table 3.1. Next, we saw that the limit on concentrating in only one direction was lower than the degree of concentration needed for our target high efficiency, especially if the angular spread entering the parallelepiped was to stay low so the trough concentrator was changed to a primary square CPC as shown in Figure 3.1b.

The simplest version of this design uses the cells themselves as absorption filters with their back-reflectors as mirrors. Broadband light enters the structure, enters the highest bandgap subcell where the above-bandgap light is absorbed. The remainder is reflected by the back reflector to the 2nd highest bandgap subcell and so on. However, in each cell there is some small amount of loss of below-bandgap energy light. Simulations were done assuming 5-10% parasitic absorption of out-of-band light. The efficiency of the structure was not high enough, so we opted to include short pass filters on the front of each of the seven solar cells. Thus the filter would reflect all out-of-band light before it entered and experienced parasitic absorption in the cell while the target band would be transmitted. The filters were designed to be short-pass filters so that any high energy light that failed to be transmitted and collected in the highest bandgap cell could still be transmitted and converted in one

of the lower bandgap cells. This way, instead of being lost completely, it might simply produce lower voltage than if collected in the correct cell. This was dubbed the Generation I design.

Designing Bragg stacks with short wavelength pass-bands which simultaneously reflected light all the way to 1676 nm for the seventh subcell with bandgap $E_g = 0.74\ eV$ proved very difficult. Decreasing angular spread on the filters improved efficiency, but there is a need for concentration for both high performance and acceptable cost. Thus the primary concentration was decreased and we incorporated secondary compound parabolic concentrators between the filter and cell creating the Generation II design which had a multipart secondary receiver at each of the seven positions as shown in Figure 3.1d. The concentrators were cut at a 45° angle for incorporation. Fabrication and characterization of the concentrators is discussed in Chapter 4. This is the Generation II PSR.

The performance of the Generation II filters was still not high enough to achieve 50% module efficiency. In response, the Gen. II filter order was modified so that the lowest bandgap subcell came first. With this changed order the first subcell was the 0.74 eV cell followed by the six other cells in order of decreasing bandgap from 2.11 eV to 0.93 eV. The first filter could then be a long-pass filter, and the second filter with the broadest reflection band must reflect from 589 nm to 1333 nm rather than 589 nm to 1676 nm in the original order.

Despite the improvement over the Generation I filter design, getting sufficient performance from the one long-pass and six short-pass filters still required many inconvenient design compromises. First, it was necessary to remove the primary concentration to reduce the angular spread on the filters. Second, without primary concentration, the only way to tile the PSR submodules into a module is via vertical offsets equal in height to the PSR height as shown in Figure 3.1c. This would in very tall, unwieldy modules. Third, the lack of a common plane for the cells meant we would need to somehow contact and heat sink seven physically separated cells. Finally, the hollow PSR cavity required high quality anti-reflection coatings for both the filters and the cells.

To address these practical and performance challenges, the Generation IV design was developed (Figure 3.1e). Given that long-pass filters are easier to make, all the filters were converted to long-pass filters placed at a 45° angle to the incident lightpath. Each reflected frequency band is directed perpendicular to the lightpath, allowing a common plane for the cells allowing easier integration. The long-pass

(a) Original Concept   (b) Generation I   (c) Vertical Offset

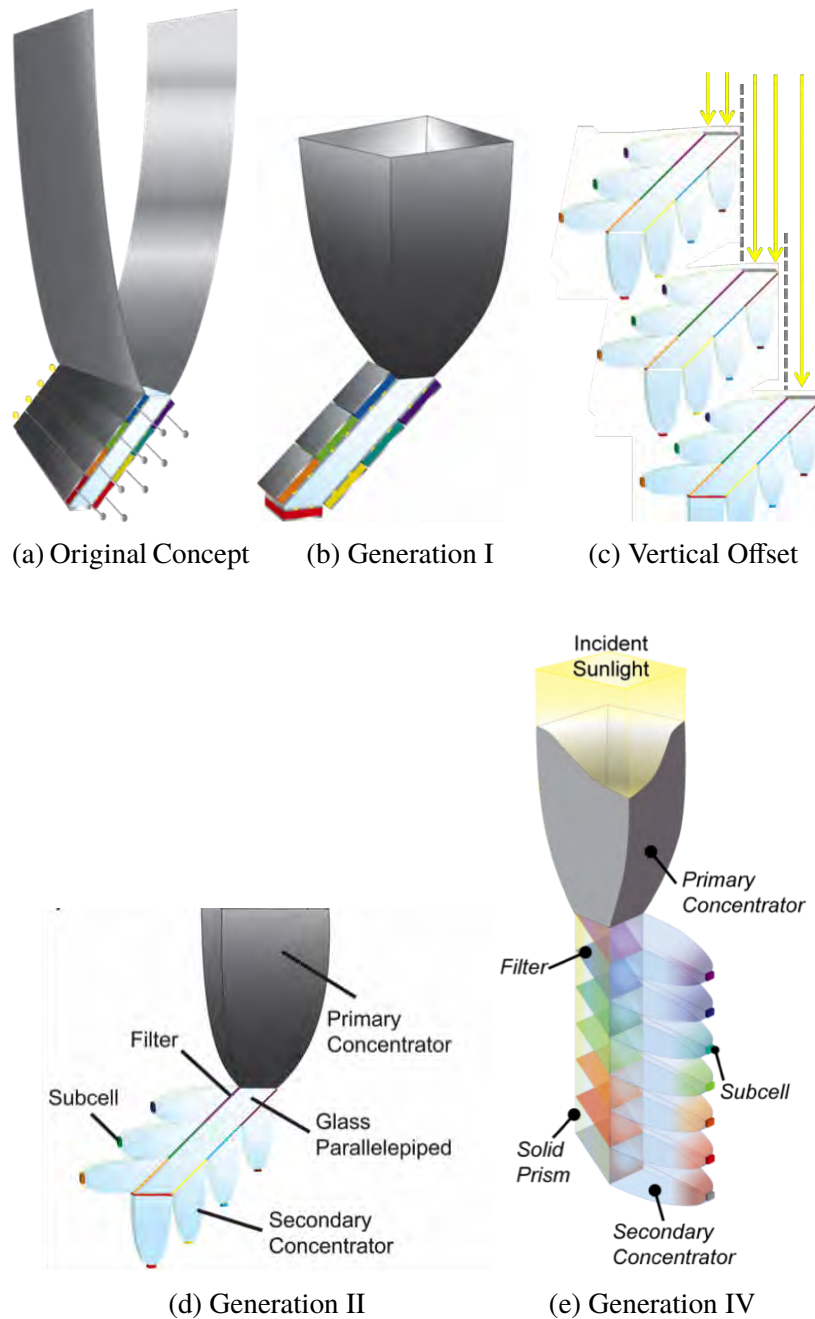(d) Generation II   (e) Generation IV

Figure 3.1: Polyhedral Specular Reflector design schematics.

filters can be designed to be embedded in an $n \approx 1.5$ medium with some degree of primary concentration simplifying ARC design and tiling of the submodules into modules. The final change made to the PSR design during prototyping was to change the secondary concentrators from PDMS CPC to glass lightpipes. This change was made because the long optical path length of PDMS absorbed too much light and finding a method or vendor to fabricate the CPC curvature in glass proved elusive.

Further design changes to make the PSR concept a viable commercial photovoltaic technology are discussed in Section 5.2.

Receiver	Subcell E_g (eV)	Gen IV filter reflection band	Subcell Alloy
1	2.11	350 – 588 nm	$Al_{0.20}Ga_{0.32}In_{0.48}P$
2	1.78	589 – 697 nm	$Ga_{0.51}In_{0.49}P$
3	1.58	698 – 785 nm	$Al_{0.1}Ga_{0.9}As$
4	1.42	786 – 873 nm	$GaAs$
5	1.15	874 – 1078 nm	$In_{0.87}Ga_{0.13}As_{0.28}P_{0.72}$
6	0.93	1079 – 1333 nm	$In_{0.71}Ga_{0.29}As_{0.62}P_{0.38}$
7	0.74	1334 – 1676 nm	$In_{0.53}Ga_{0.47}As$

Table 3.1: Wavelength range of spectral bands for the PSR design and Generation IV design filter specifications

Coupled Optoelectronic Model

In order to get a full sense of the efficiency potential of the PSR, our team coupled a series of simulation tools. Dr. Emily Warmann used available databases of solar resource data including the NREL Simple Model of the Atmospheric Radiative Transfer of Sunshine (SMARTS) resource [29] and National Solar Radiation Database (NSRDB) [30] to create a dataset of 365 days of annual solar irradiance in a variety of locations across the US to estimate annual energy production. [6] Dr. Carissa Eisler used an open-source transfer matrix method optimization software OpenFilters to design Bragg stacks for the PSR as well as anti-reflection coatings (ARC) for each of the seven solar cells. [31] The filter and ARC optical characteristics were then integrated into a ray tracing program (LightTools) to optimize the degrees of primary and secondary concentration and to determine the incident photon flux on each solar cell in the integrated PSR. The spatial distribution of the photon fluxes were used by Cris Flowers using an HSPICE based distributed circuit model to design an electrical contact grid to minimize fraction of the solar cells shadowed by the metallic front contacts while also limiting series resistance losses. The resulting data for integrated device peak efficiency and annual energy production were used to evaluate our progress toward 50% module efficiency. Additionally, these technical data were used in conjunction with cost modeling, described in Chapter 5, to project $/W and LCOE for the PSR at high-volume production.

PSR Prototypes

We made a number of prototypes of the PSR design throughout the project. The first two were prototypes of the Generation I design, made with six of the seven

intended subcells (all but the 0.74 eV). This was done using commercially available long-pass filters. The cells were designed using open-source 1D device physics solver AFORS-HET [32], were grown by a semiconductor and were processed into devices at Caltech. The prototype efficiency measured 11%. Figure 3.2a shows this design. Generation 2 was not prototyped, and only partial prototypes were made of the Generation III design. Figure 3.2b shows a 3D printed mechanical prototype of Generation III. The green collars connect the CPC tips to photodiodes mounted on small, yellow pieces of printed circuit board which would both mechanically support the cell and allow for electrical interconnections. Figure 3.2c shows a partial optical prototype of this design. The first long-pass filter and the first two short pass filters are shown with concentrators attached. Normally incident red and green light from laser pointers is appropriately separated. The green light is reflected off the longpass filter, passed through the second filter, and concentrated where the 2.1 eV cell would be in a full prototype. Likewise, the red laser light is predominantly reflected by the first two filters and passed into the third concentrator. The fact that the laser beam paths are visible going through the concentrator is indicative of surface and volume scattering.

Three Generation IV prototypes have been built, and the final prototyping effort is currently underway at the time of writing. The solar cell epitaxial layer growth was done by Boeing Spectrolab while processing of wafers into devices including epitaxial lift-off was done in our labs by John Lloyd. The optical path was composed of six parallelepiped pieces with filters deposited on one face each and a seventh triangular piece to give the flat input aperture. These seven pieces were each masked using Kapton tape and adhered using PDMS. The tape prevented the PDMS from running up the sides of the structure creating scattering points for light that should be totally internally reflected at optically smooth interfaces. A similar tape masking and PDMS gluing process was used to attach the seven concentrators to the appropriate faces of each parallelepiped piece after the main optical splitting structure had been assembled, resulting in the prototype shown in Figure 3.2d. The optical characterization results for the PSR train with 194X PDMS secondary concentrators and 1.7X primary concentrator are shown in Figure 3.3. While the filter train alone has high optical efficiency, the PDMS concentrator efficiency is 60-70% and the integrated CPC have alignment errors contributing additional losses. The overall optical efficiency of this structure is thus slightly above 60%.

The next Generation IV prototype used 16X glass lightpipes (Figure 3.2e), which

gave much higher optical efficiency than PDMS CPC. The incident photon collection efficiency averaged 73%. Its spectral dependence was also very flat as shown in Figure 3.4. The overall submodule efficiency was found to be 22.9%. Losses included a variety of optical, cell and integration related issues. The cell voltages and degree of concentration were lower than simulated. Due to all seven subcells not yet being ready, 0.74 eV bandgap cells were incorporated at each of three lowest bandgap locations, and similarly a 1.54 eV cell in place of the intended 1.78 eV cell.

Many of these concerns were addressed in the most recent prototype which used 100X long lightpipes in place of the 16X short lightpipes (Figure 3.2f). However, the small size of the subcells created a new loss source. The alignment of the 1 mm^2 subcells at the bottom of the 10 cm long lightpipes proved difficult, and misalignment and light leakage at the cell-PDMS-lightpipe interface decreased photon collection to 53%. Thus, despite incorporating the seven correct subcells which much improved performance, the overall submodule efficiency dropped slightly to 22.4%. The simulated efficiency of the long lightpipe PSR with subcells hitting their performance targets is 47%. The current prototyping effort incorporates improved cells as well as an improved alignment procedure for attaching the subcells to the end of the 100X lightpipes. Hopefully this last prototype will far surpass the previous prototypes and approach or beat today's spectrum splitting submodule efficiency record of 38.5%. [9]
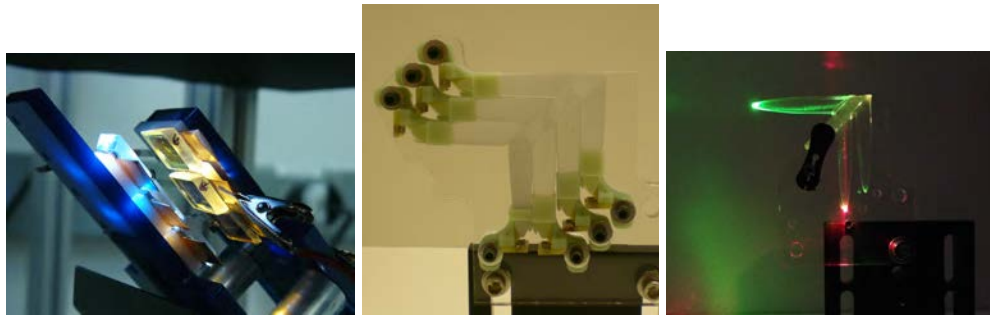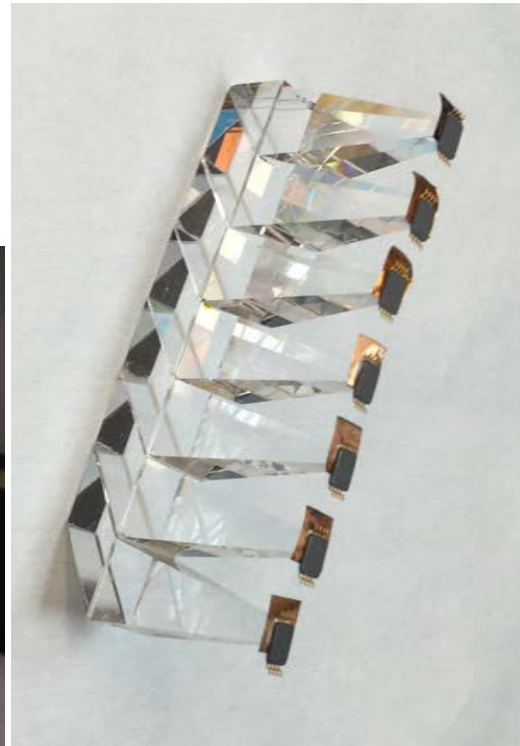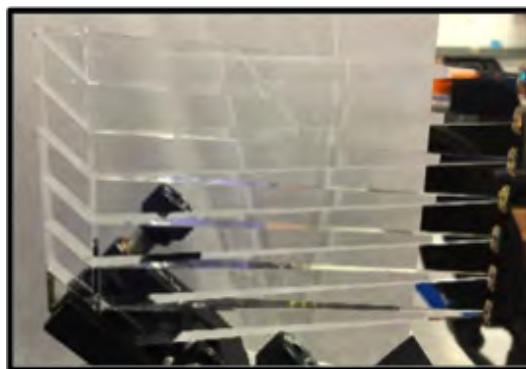
(a) Gen I
(b) Generation III
(c) Generation III

(d) Gen. IV with PDMS CPC
(e) Gen. IV with short glass lightpipes

(f) Generation IV with long lightpipes

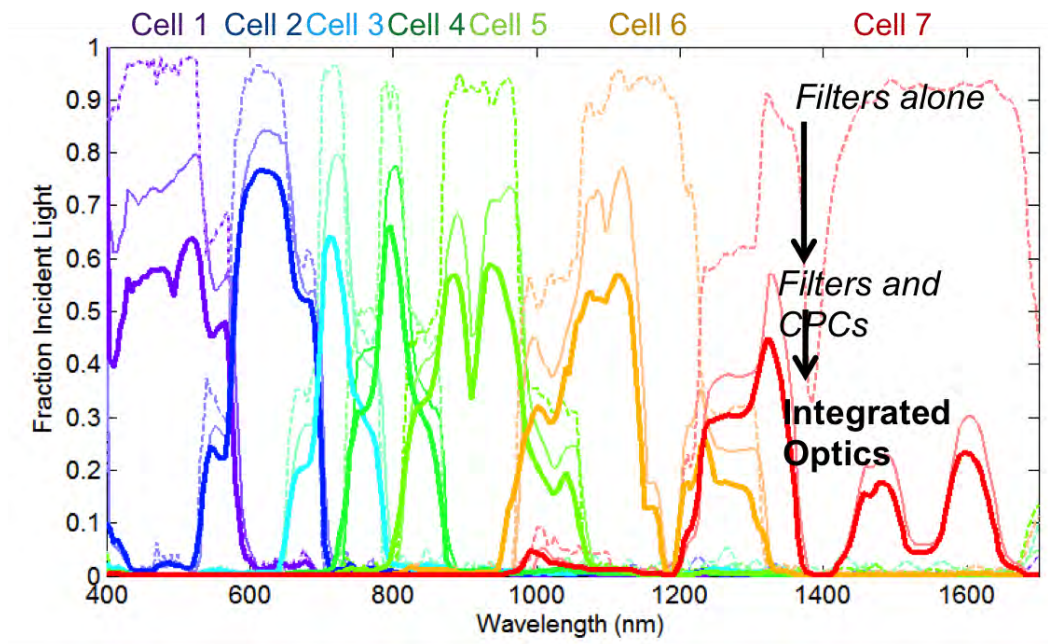Figure 3.2: Polyhedral Specular Reflector prototype photographs.

Figure 3.3: Polyhedral Specular Reflector with PDMS CPC optical characterization results. © 2015 IEEE
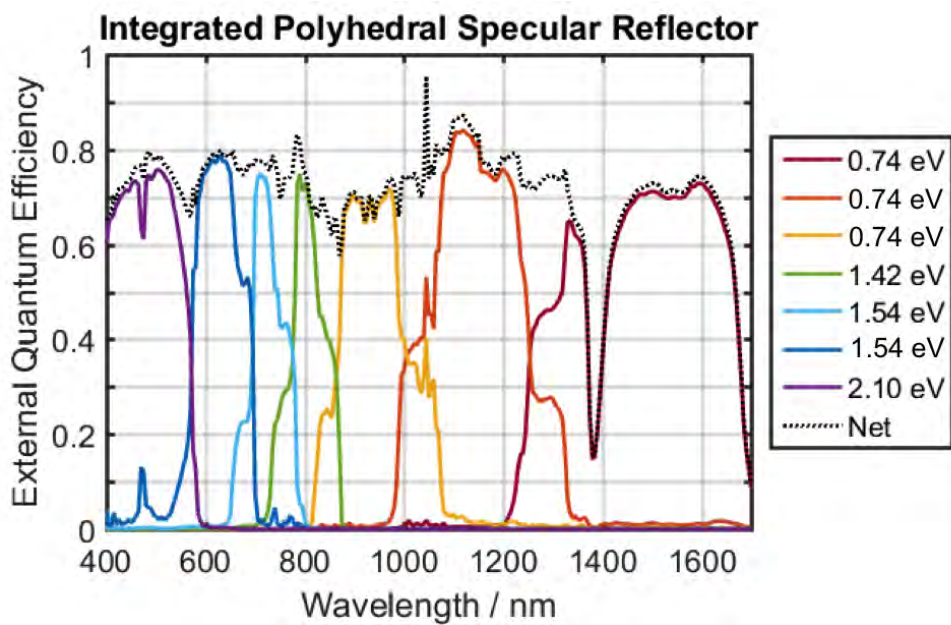

Figure 3.4: Polyhedral Specular Reflector with short lightpipes full device external quantum efficiency.